PCCP

PAPER

View Article Online
View Journal | View Issue

Cite this: *Phys. Chem. Chem. Phys.*, 2018, **20**, 26846

C–O bond activation and splitting behaviours of CO_2 on a 4H-SiC surface: a DFT study†

Dandan Wang,[a] Liangliang Zhang,[*b] Dongxue Han,[cd] Li Niu,[cd] Xin Zhong,[a] Xin Qu,[a] Lihua Yang,[a] Jialong Zhao[a] and Haibo Li*[a]

Received 13th July 2018,
Accepted 8th October 2018

DOI: 10.1039/c8cp04438d

rsc.li/pccp

Conversion of CO_2 into valuable chemicals can not only reduce the amount of CO_2 in the atmosphere, but also realize the reuse of resources. It's well known that C–O bond activation and splitting are critical steps in the CO_2 conversion process and it's crucial to employ an appropriate catalyst. Here, the adsorption and activation behaviors of a CO_2 molecule on 4H-SiC surfaces were systematically investigated based on DFT calculations. Calculation results show that the CO_2 molecule can anchor on 4H-SiC(0001) and (000$\bar{1}$) surfaces. On the 4H-SiC(0001) surface, the adsorbed CO_2 molecule prefers to dissociate with an energy barrier of 0.52–0.70 eV, producing an O adatom and a CO molecule on the surface. Further dissociation of the CO is hindered due to a large energy barrier of 2.12 eV. However, if a H atom is introduced, the CO molecule may combine with H into a CHO group and the reaction energy barrier is 1.69 eV. Moreover, the CHO group tends to transform into a CH group and an O adatom, a reaction in which a relatively low energy barrier of 0.09 eV needs to be surmounted. For the 4H-SiC(000$\bar{1}$) case, the direct C–O bond dissociation energy barrier for CO_2 is only 0.37 eV while further breaking of the C–O bond in CO is energetically unfavorable even with the help of a H atom. So the final products are an O adatom and CO chemisorbed on the 4H-SiC(000$\bar{1}$) surface. All the calculation results demonstrate that the inert CO_2 molecule can be effectively activated on both the 4H-SiC(0001) and (000$\bar{1}$) surfaces and different splitting products could be obtained on the two different surfaces, implying that SiC is an applicable catalyst material for CO_2 conversion with high efficiency and product selectivity.

1. Introduction

The reduction in the use of fossil fuels and the decrease of atmospheric CO_2 level has drawn a lot of attention in the last few years. On the one hand, CO_2 is the main cause of global warming. To reduce the CO_2 level, an accepted effective strategy is carbon capture and sequestration at large sources of emission such as at heating and power stations.[1,2] However, there are two serious problems in the technology involved, including the high cost and the uncertainty of whether the technology really works. On the other hand, CO_2 is an abundant, cheap, and safe raw chemical material, which could be converted into high value added chemicals and even liquid fuels, such as carbon monoxide, methanol, and even gasoline fuels.[3,4] This can not only reduce the amount of CO_2 in the atmosphere, but also realize the reuse of resources and generate huge benefits in both the environment and for energy. So the recovery and catalytic conversion of CO_2 is regarded as the most promising solution for the CO_2 problem.

At present, there is a large number of reports on the investigation of CO_2 catalytic conversion. As early as 1991, deep research on the CO_2 catalytic reforming of CH_4 began. In the reforming process, a syngas of CO and H_2, in the ratio of 1 : 1 is produced and these are the ideal raw materials for carboxyl and feto synthesis.[5] As a reducing agent, H_2 has a convenient source, and catalytic hydrogenation is an efficient technology for CO_2 utilization. It has been reported that by controlling the degree of reduction, different products can be obtained. Over the last couple of years, the catalytic conversion of industrial CO_2 waste gas into liquid fuels with H_2 has become a hot topic in the field of CO_2 catalytic conversion.[6–8] The photocatalytic reduction of CO_2 has always been given intensive attention since it was first reported in 1979.[9,10] In this process, the

[a] *Key Laboratory of Functional Materials Physics and Chemistry of the Ministry of Education, Jilin Normal University, Siping 136000, China. E-mail: lihaibo@jlnu.edu.cn*
[b] *State Key Laboratory of Luminescence and Applications, Changchun Institute of Optics, Fine Mechanics and Physics, Chinese Academy of Sciences, 3888 Eastern South Lake Road, Changchun 130033, China. E-mail: Zhangliangliang@ciomp.ac.cn*
[c] *Center for Advanced Analytical Science, School of Chemistry and Chemical Engineering, Guangzhou University, Guangzhou 510006, P. R. China*
[d] *State Key Laboratory of Electroanalytical Chemistry, c/o Engineering Laboratory for Modern Analytical Techniques, Changchun Institute of Applied Chemistry, Chinese Academy of Science, Changchun, 130022, China*

† Electronic supplementary information (ESI) available. See DOI: 10.1039/c8cp04438d

photo-generated electrons in the photocatalyst possess strong reduction properties, they are utilized to reduce CO_2 into fuels or chemical raw materials, with the help of H_2O. What's more, the investigation of electrocatalytic CO_2 reduction can be traced back to the 19th century. This technology utilizes renewable energy sources (solar, wind, or surplus nuclear power) and the required hydrogen is obtained from a electrolytic water process. The mild conditions of the whole reaction gives this method wide application prospects and potential.[11–13]

In spite of the fact that plenty of efforts have been made and some results have been obtained for CO_2 catalytic conversion, many problems still exist and further study is needed for real applications. For example, the high energy consumption in CO_2 catalytic reforming and catalytic hydrogenation limits their large-scale application in industry. From the view point of energy consumption, the research direction of CO_2 catalytic conversion should be focused on reactions under mild conditions, such as photocatalytic and electrocatalytic reduction. In photo- and electro-catalytic reduction, the choice of catalyst is crucial and the catalytic performance of almost all of the catalysts needs to be improved.[14,15] Moreover, under the action of different catalyst materials and reaction conditions, the reduction products are varied, including CO, CH_4, HCOOH, CH_3OH and even long chain of hydrocarbons.[16–18] Therefore, catalyst materials with high catalytic activity, high product selectivity, and high stability are essential.

In recent years, various catalyst materials have been developed, such as noble metals,[19,20] transition metal oxides,[21,22] two-dimensional nanomaterials,[23,24] and so on. Nowadays, SiC, as an non-metallic oxide catalyst, has been paid more and more attention in the area of photo- and electro-catalysis. For example, He *et al.* reported that ultrathin 3C-SiC nanocrystals were highly efficient in electrochemical hydrogen evolution because of the surface autocatalytic effect.[25] Recently, one of the most important applications of SiC is that it has also been demonstrated to possess high photocatalytic activity for CO_2 reduction.[26] These reports demonstrate that SiC possesses a high surface activity which is essential in the application of heterogeneous catalysis.

In this work, the adsorption and splitting behaviors of a CO_2 molecule on a SiC surface, which are the most important steps for CO_2 surface catalysis, are investigated from the theoretical side. In the calculation design, two different surfaces, the 4H-SiC(0001) and $(000\bar{1})$ surfaces, were chosen. On the 4H-SiC(0001) surface, the adsorbed CO_2 molecule tends to dissociate directly into an O adatom and a CO molecule chemisorbed on the surface. Then the CO would combine with H into CHO group which finally transforms to a CH group and an O adatom. On the 4H-SiC$(000\bar{1})$ surface, the direct dissociation of CO_2 is both thermodynamically and dynamically favorable, while further breaking the C–O bond of CO is energetically unfavorable even with the help of a H atom. These results may give a clear understanding of CO_2 adsorption and activation on 4H-SiC surfaces and provide proposals for the further application of 4H-SiC in CO_2 selective catalytic conversion.

2. Computational methods

Our theoretical calculations were performed based on density functional theory (DFT) within the Perdew–Burke–Ernzerhof (PBE) generalized gradient approximation and the projected augmented wave (PAW) method as implemented in the VASP package.[27,28] For the structure optimizations, a Monkhorst–Pack grid of $9 \times 9 \times 2$ *K*-points was applied for the Brillouin-zone integration for the SiC bulk unitcell. For SiC surface supercells and adsorption systems, the *K*-point samplings were set as $3 \times 3 \times 1$. Atomic positions were relaxed until their residual forces were less than 0.01 eV $Å^{-1}$ for bulk relaxation and less than 0.03 $Å^{-1}$ for surface relaxation. The cutoff energy for the plane wave basis was set as 400 eV in all the calculations. The calculated lattice constants of 4H-SiC are $a_0 = b_0 = 3.089$ Å and $c = 10.114$ Å, in nice agreement with experimental values.[29] Both the 4H-SiC(0001) and $(000\bar{1})$ surfaces were represented by eight atomic-layer slabs with a lateral size of $a = b = 9.27$ Å, as shown in Fig. 1. A vacuum region of 13 Å was used along the direction perpendicular to the slab in building the surface supercells to avoid the interaction between two adjacent periodic images. For surface optimizations, the top four atom positions were relaxed while the bottom four layers were kept fixed to their bulk positions.

The adsorption energies are calculated according to the equation $E_{ads} = E_{CO_2/surface} - (E_{surface} + E_{CO_2})$, where $E_{CO_2/surface}$, $E_{surface}$ and E_{CO_2} are the total energies of the surface with the adsorbed CO_2 molecule, the clean surface and the isolated CO_2 molecule, respectively.[30] Whereafter, the activation and dissociation pathways of the adsorbed CO_2 molecules were investigated using the climbing image nudged elastic band (Cl-NEB) method implemented in VASP.[31,32] Frequency analysis has been carried out to make sure the TS structures are the real TS.

3. Results and discussion

3.1 Adsorption and dissociation of CO_2 on the 4H-SiC(0001) surface

To determine the stable adsorption configurations of CO_2 on the 4H-SiC(0001) surface, all possible configurations were systematically studied. Based on the total energy calculations,

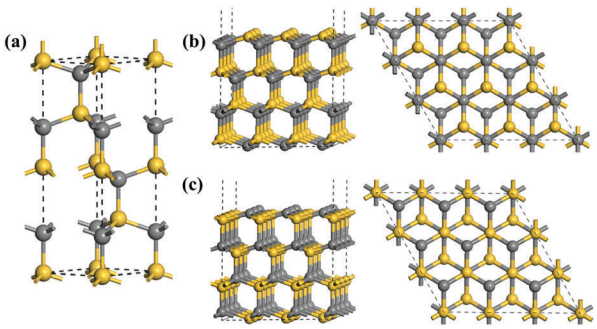

Fig. 1 Relaxed geometry structures of (a) the 4H-SiC bulk, (b) the 4H-SiC(0001) surface, and (c) the 4H-SiC$(000\bar{1})$ surface. The yellow and gray balls represent the Si and C atoms, respectively.

four stable chemisorption configurations were verified. As can be seen in Fig. 2(d), in the most stable configuration, all the three atoms of the CO_2 molecule bond with the surface Si atoms with an adsorption energy of −3.30 eV. This configuration is often referred to as the tridentate configuration.[33] The corresponding bond lengths of newly formed O–Si and C–Si bonds are 1.747 Å, 1.740 Å and 1.940 Å. What's more, the two C–O bonds of CO_2 molecule are lengthened from 1.176 Å (C–O bond length of the isolated CO_2 molecule) to 1.372 Å and 1.378 Å, signifying C–O bond activation and the great possibility of CO_2 splitting.

The second stable adsorption state (Fig. 2(c)) is also a tridentate configuration and the adsorption energy is −3.15 eV. The only difference between these two adsorption configurations is that they originated from different adsorption sites. In Fig. 2(d), the C atom of the CO_2 molecule occupies the hollow center site of the Si–C hexatomic ring. While as shown in Fig. 2(c), the C atom of the CO_2 molecule takes up the position of a C atom as in the subsurface atomic layer. The two newly formed O–Si bonds possess the same bond length of 1.765 Å and the newly formed C–Si bond length is 1.965 Å. Both the two C–O bonds of the CO_2 molecule are 1.362 Å, which is 0.186 Å longer than those of the isolated CO_2 molecule.

CO_2 can also chemisorb on the SiC(0001) surface with only two newly formed bonds as presented in Fig. 2(a) and (b), with the adsorption energy of −2.14 eV and −3.19 eV respectively. In Fig. 2(a), both the two O atoms of the CO_2 molecule bond to the surface Si atoms with newly formed O–Si bond lengths of 1.719 Å, and the two C–O bonds of CO_2 molecule are enlarged to 1.354 Å and 1.355 Å. In Fig. 2(b), one of the two O atoms and the C atom of the CO_2 molecule bond with two surface Si atoms. The bond lengths of the newly formed C–Si bond and O–Si bond are 1.979 Å and 1.709 Å respectively, and the two C–O bond lengths of the molecule are 1.203 Å and 1.436 Å. Based on the difference charge density plots presented in Fig. S1 (ESI†), obvious charge redistribution occurs in the adsorbed state. CO_2 is activated due to the charge transfer from the SiC(0001) surface to it and this adsorption configuration can be referred to as bent $CO_2^{\delta-}$.[33] Further Bader charge analysis denotes that δ = 1.42.

Comparing the adsorption structures and the adsorption energies, we found that the tridentate configuration may be transformed from that in Fig. 2(a). The transformation barriers and the corresponding transition states from Fig. 2(a)–(d) are further studied and presented in Fig. S2 (ESI†). Cl-NEB results revealed that the transformation barrier is only 0.23 eV.

Following this, we investigated the splitting behaviors starting with the tridentate CO_2 in Fig. 2(b) and the $CO_2^{\delta-}$ in Fig. 2(d). To determine the adsorption configurations of the splitting intermediates and products, all possible configurations were systematically studied and the most stable configurations are presented and considered in this text. In order to understand the activation and dissociation processes of CO_2 more clearly and with intuitive understanding, a simplified reaction process is presented in Fig. 8. As presented in Fig. 3, the splitting of CO_2 is an exothermic process with two transition states. The overall reaction barrier for the splitting of $CO_2^{\delta-}$ is 0.18 eV lower than that for the tridentate configuration. This can be explained by the slightly longer bond length of the C–O bond in $CO_2^{\delta-}$. For $CO_2^{\delta-}$, the first barrier is 0.52 eV and the second barrier is only 0.38 eV, both are easily surmounted. The energy change between the initial and final state is −0.48 eV. Comparing the structures and bond lengths of the transition states with the initial and final states, both the two transition states of TS1 and TS2 are more product-like than reactant-like. For the tridentate CO_2, the two energy barriers are 0.70 eV and 0.44 eV, and the energy change between the initial and final states is −0.34 eV. TS1 is more reactant-like than product-like, while TS2 is more product-like than reactant-like. In any case, the CO_2 splitting into an O adatom and chemisorbed CO on the SiC(0001) surface happens easily. The further dissociation of CO on the SiC(0001) surface has also been studied. However, Fig. 3(a) indicates that the direct dissociation energy barrier of CO is as high as 2.12 eV, meaning the CO splitting is dynamically unfavorable.

Moreover, in order to estimate the contributions by vdW physical interactions to the CO_2 adsorption systems, the van der Waals DFT-D2 correction method of Grimme[34] was applied. The strength of the vdW physical interaction is defined as $\Delta E = E_{ads}(\text{vdW}) - E_{ads}(\text{novdW})$, where $E_{ads}(\text{vdW})$ and $E_{ads}(\text{novdW})$ are the adsorption energies with and without DFT-D2 correction, respectively. The corresponding values of ΔE are listed in Table 1. Obviously, the vdW interaction affects the adsorption

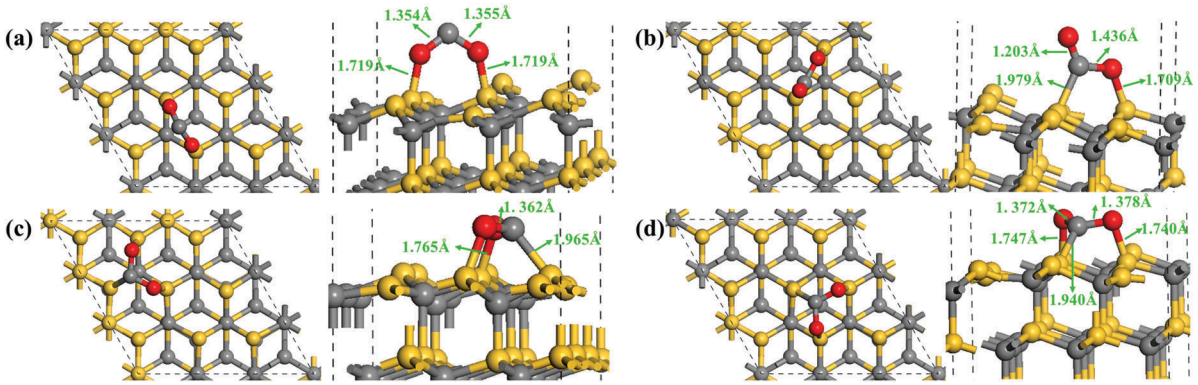

Fig. 2 The side and top views of the chemisorption configurations of CO_2 molecules on the SiC(0001) surface. From (a)–(d), adsorption energy increases. Gray, red and yellow balls denote the C, O and Si atoms, respectively.

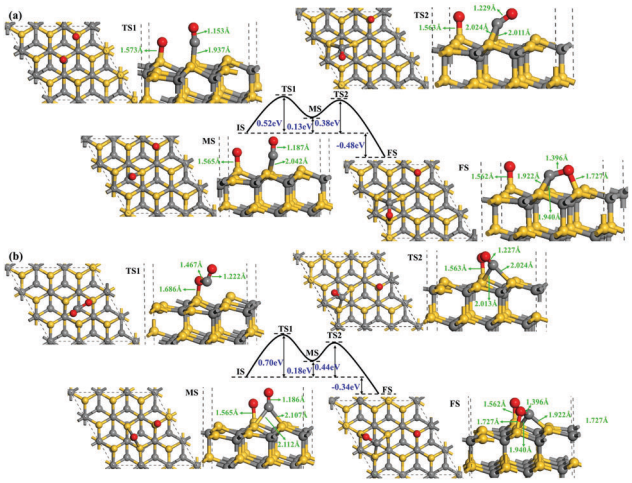

Fig. 3 (a) The minimum energy path for CO_2 splitting, the initial configuration is that shown in Fig. 2(b); (b) the minimum energy path for CO_2 splitting, the initial configuration is that shown in Fig. 2(d). To save space, the initial structures in the Cl-NEB paths are not repeatedly shown here. The gray, red and yellow balls represent the C, O and Si atoms, respectively.

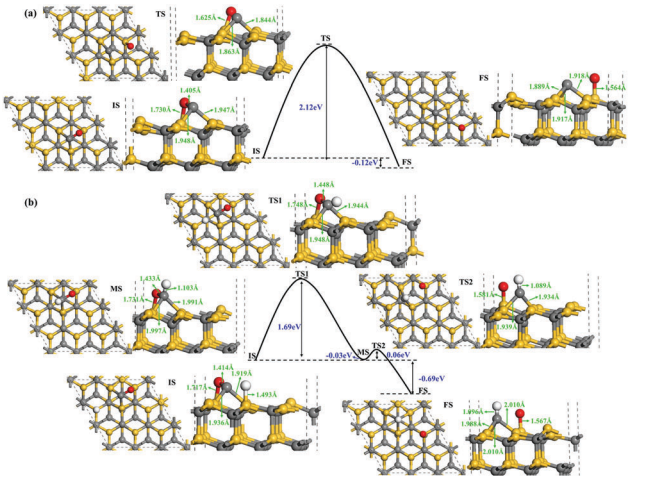

Fig. 4 (a) The minimum energy path for CO dissociation; (b) the minimum energy path for CO dissociation with the help of a H atom. The gray, red, yellow and H balls represent the C, O, Si and H atoms, respectively.

energies significantly. Then the transformation of CO_2, including the vdW correction from the adsorption configuration in Fig. 2(a) to that in Fig. 2(d), was investigated to further evaluate the vdW interaction influence on the Cl-NEB processes. The transformation barriers and the corresponding transformation path from Fig. 2(a)–(d) with and without the vdW correction are consistent, as shown in Fig. S3 (ESI†). These results indicate that the vdW correction produces little effect on the Cl-NEB energy barriers and therefore the vdW interactions are ignored in other Cl-NEB reaction processes.

CO_2 adsorption in the presence of a H atom was also investigated in this work because hydrogen is a necessary element in the CO_2 conversion process. Four possible structures were considered, CO_2 + H co-adsorption, COOH group adsorption, HCOO group adsorption, and CO + OH co-adsorption, and are shown in Fig. S4 (ESI†). The results demonstrated that for $CO_2^{\delta-}$, the HCOO and COOH groups are energetically unfavourable while the CO + OH co-adsorption is thermodynamically favourable. For the tridentate CO_2, the HCOO group and the CO + OH co-adsorption structures are thermodynamically favourable. It is worth noting that by comparing all of the total energies of the CO_2 + H co-adsorption, COOH group, HCOO group and CO + OH co-adsorption, the HCOO group is thermodynamically favorable. However, it is unfavorable in terms of kinetics because the reaction barrier from CO_2 + H co-adsorption to the HCOO group is as high as 2.17 eV, as shown in Fig. S5 (ESI†).

Then, the H influence on CO_2 and CO splitting was studied. The calculation results presented in Fig. 5 show that H will suppress CO_2 splitting due to the big increase of the reaction barriers. Nevertheless, H influence on CO dissociation is positive. We can see from Fig. 4(b) that the energy barrier of CO dissociation with the help of a H atom is lowered to 1.69 eV and the final products are an O adatom and a CH group chemisorbed on the surface. Notably, there is a middle state of the CHO group along the reaction path and the transition energy barrier from CHO to the CH + O state is only 0.09 eV. In addition, the possibility of forming the H_2CO^* from CHO and H was studied. The reaction barrier is as high as 2.39 eV and the reaction is endothermic with a reaction energy of 1.26 eV. So the reaction is unfavorable in view of thermodynamics and kinetics in comparison with the HCO splitting reaction. However, CH in principle is not a very stable intermediate; the reaction may not stop at this step. We investigated several possible reactions including CH + CH → C_2H_4, CH + H → CH_2, CH_2 + H → CH_3, CH_2 + CH_2 → C_2H_4, CH_3 + CH_3 → C_2H_6 and CH_3 + H → CH_4. Unfortunately, the reaction barriers for forming C_2H_4, CH_2 and CH_3 are around 2.0 eV and all the reactions are endothermic. In order to get the final product, other improvement measures need to be introduced and further research involved in the product design is needed.

Table 1 The calculated adsorption energies of the CO_2 molecules on the SiC surfaces and the corresponding values of the vdW interaction strength

SiC surface	Configuration	E_{ads}(novdW)	E_{ads}(vdW)	ΔE
(0001)	Fig. 2(a)	−2.14	−2.77	0.63
	Fig. 2(b)	−3.19	−3.51	0.32
	Fig. 2(c)	−3.15	−3.49	0.35
	Fig. 2(d)	−3.30	−3.67	0.37
(000$\bar{1}$)	Fig. 6(a)	−0.90	−1.12	0.22
	Fig. 6(b)	−0.43	−0.71	0.28
	Fig. 6(c)	−0.23	−0.54	0.31
	Fig. 6(d)	−1.51	−1.78	0.27

3.2 Adsorption and dissociation of CO_2 on the 4H-SiC(000$\bar{1}$) surface

Fig. 6 presents the optimized structures of the CO_2 adsorption states on the SiC(000$\bar{1}$) surface. In the configuration shown in Fig. 6(a) which can also be labeled as $CO_2^{\delta-}$, one of the two O atoms of the CO_2 molecule bonds with the subsurface

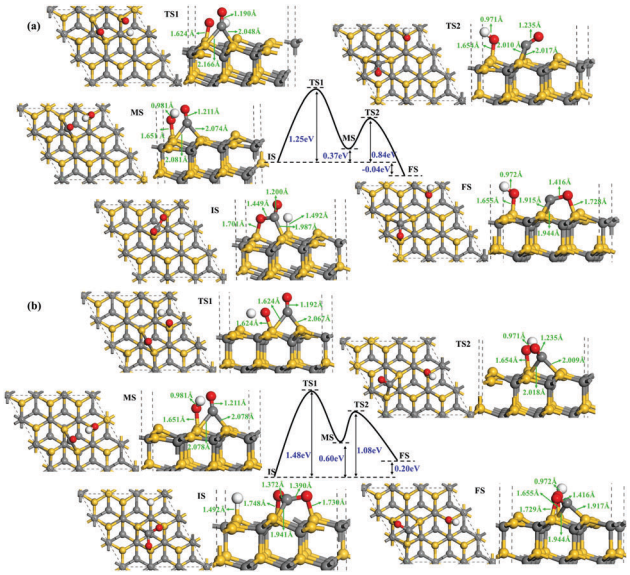

Fig. 5 The minimum energy path for transformation from the CO_2 + H co-adsorption to the CO + OH co-adsorption group: (a) for the CO_2 adsorption state in Fig. 1(b) and (b)for the CO_2 adsorption state in Fig. 1(d). The gray, red, yellow and white balls represent the C, O, Si and H atoms, respectively.

Si atom and the C atom of the CO_2 bonds with the surface C atom with the adsorption energy of −0.90 eV. The corresponding bond lengths of the newly formed O–Si and C–C bonds are 1.752 Å and 1.535 Å, and the two C–O bonds of CO_2 molecule are lengthened to 1.378 Å and 1.214 Å. The adsorption states in Fig. 6(b) and (c) possess tridentate configurations. In Fig. 6(b), the C atom of the CO_2 molecule occupies the hollow center site of the Si–C hexatomic ring with the adsorption energy of −0.43 eV. All three atoms of the CO_2 molecule bond with three surface C atoms and the newly formed C–O and C–C bond lengths are 1.582 Å, 1.588 Å and 1.440 Å. The two C–O bonds of the CO_2 molecule are lengthened to 1.362 Å and 1.363 Å. While in Fig. 6(c), the adsorption energy is only −0.23 eV and the C atom of the CO_2 molecule takes up the position of a Si atom on top of the subsurface Si atom. The corresponding bond lengths of the newly formed C–O, C–C

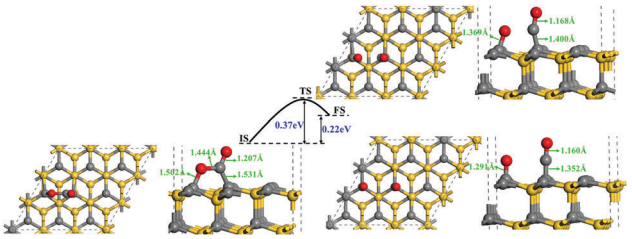

Fig. 7 The minimum energy path for CO_2 splitting. The gray, red and yellow balls represent the C, O and Si atoms, respectively.

bonds and C–O bonds of the CO_2 molecule are 1.571 Å, 1.562 Å, 1.431 Å, 1.370 Å and 1.371 Å respectively. The $CO_2^{\delta-}$ configuration in Fig. 6(d) is the most stable adsorption state with an adsorption energy of −1.51 eV. In this structure, one of the two O atoms and the C atom of CO_2 molecule bond with two surface C atoms, with newly formed O–C and C–C bond lengths of 1.502 Å and 1.531 Å. Correspondingly, the C–O bonds in the CO_2 molecule are enlarged to 1.444 Å and 1.207 Å.

Analogous to the CO_2 adsorption on the 4H-SiC(0001) surface, transformation may occur among the adsorption configurations on the 4H-SiC(000$\bar{1}$) surface. We found that the adsorption configurations in Fig. 6(a)–(c) may transform into the configuration Fig. 6(d). The transformation barriers and the corresponding transition states of the adsorption configuration transformations are presented in Fig. S6 (ESI†), in which the energy barriers are only 0.51 eV and 0.11 eV. Considering the structural similarity between Fig. 6(b) and (c), the transformation path from the configuration Fig. 6(c) to (d) was not calculated.

CO_2 splitting on the SiC(000$\bar{1}$) surface was studied with the IS of $CO_2^{\delta-}$ in Fig. 6(d) and the FS of the O adatom and CO molecule chemisorbed on the surface. As shown in Fig. 7, the splitting of CO_2 is an endothermic process and the energy change between the IS and FS is 0.22 eV. However, the reaction barrier is only 0.37 eV, lower than those for CO_2 splitting on the SiC(0001) surface. The structures and bond lengths of the TS are more close to those of the FS, so the TS is more product-like than reactant-like. What's more, the CO dissociation on the SiC(000$\bar{1}$) surface is thermodynamically not allowed due to the significant energy gain of 2.66 eV from CO to C + O co-adsorption.

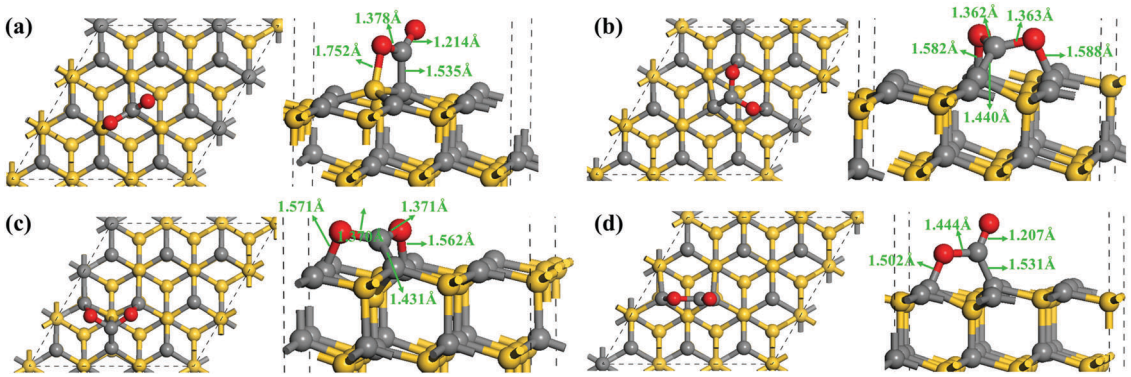

Fig. 6 The side and top views of the chemisorption configurations for the CO_2 molecules on the SiC(000$\bar{1}$) surface. Gray, red and yellow balls denote the C, O and Si atoms, respectively.

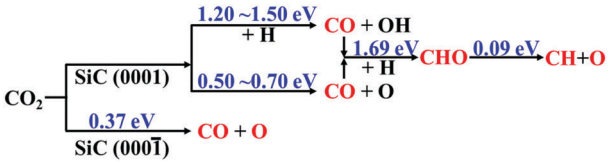

Fig. 8 Reaction path of CO_2 dissociation process on the SiC(0001) and (000$\bar{1}$) surface. The numbers in blue represent the activation energies and the possible dissociation products are marked in red.

The optimized CO chemisorption and C + O co-adsorption configurations on the SiC(000$\bar{1}$) surface are shown in Fig. S7(c) (ESI†).

We then considered H influence on the CO_2 and CO splitting on the 4H-SiC(000$\bar{1}$) surface. Based on the total energy calculations, we found that the CO_2 and H atom tend to co-adsorb on the surface instead of coupling into the COOH group, OCHO group or CO + OH co-adsorption states. The relative energies of the different adsorption states are displayed in Fig. S7(a) (ESI†). For the CO + H case, as shown in Fig. S7(b) (ESI†), the CO + H co-adsorption state is far more stable than the CHO and CH + O state. The results imply that the H atom won't facilitate the reaction of the CO_2 splitting and the CO dissociation, and the products of the CO_2 splitting on the 4H-SiC(000$\bar{1}$) surface are an O adatom and CO molecule. Similarly, the reaction process for the CO_2 splitting on the SiC(000$\bar{1}$) surface is simplified in Fig. 8.

4. Conclusions

In summary, CO_2 activation and splitting has been systematically investigated based on first-principles calculations. The results demonstrate that the CO_2 molecule is effectively activated and tends to split into a CO molecule and an O adatom on the 4H-SiC(0001) surface with a low energy barrier, lower than 0.70 eV. Without a H atom, the CO_2 splitting products will be an O adatom and a CO molecule adsorbed on surface. While under the influence of a H atom, the final products will be a CO molecule, CHO group, CH group and an O adatom. For the case of CO_2 adsorption and splitting on the 4H-SiC(000$\bar{1}$) surface, the C–O bond is also effectively activated and the splitting energy barrier is only 0.37 eV. However, whether the H atom is present or not, the CO_2 splitting products are only an O adatom and a CO molecule adsorbed on the surface. These results explain the activation and splitting mechanism on the 4H-SiC surface, which will provide a feasible strategy in the application of CO_2 catalytic conversion with high efficiency and product selectivity.

Conflicts of interest

There are no conflicts to declare.

Acknowledgements

This work was supported by the National Natural Science Foundation of China (Grant No. 11604330, 21622509, 21475122, 21527806), the Natural Science Foundation of Jilin province (Grant No. 20160520171JH), the Jilin Province Development and Reform Commission (2016C014 and 2017C053-1), and the Science and Technology Bureau of Changchun (15SS05).

References

1 J. R. Fanchi and C. J. Fanchi, Energy in the 21st Century, World Scientific Publishing Co Inc., p. 350, ISBN 9789813144804. Retrieved 27 June 2017.
2 IPCC Special Report Carbon Dioxide Capture and Storage Summary for Policymakers (PDF). Intergovernmental Panel on Climate Change. Retrieved 2011-10-05.
3 G. Centi and S. Perathoner, *Catal. Today*, 2009, **148**, 191–205.
4 C. S. Song, *Catal. Today*, 2006, **115**, 2–32.
5 A. T. Ashcroft, A. K. Cheetham, M. L. H. Green and P. D. F. Vernon, *Nature*, 1991, **352**, 225–226.
6 H. Kierzkowska-Pawlak, P. Tracz, W. Redzynia and J. Tyczkowski, *J. CO2 Util.*, 2017, **17**, 312–319.
7 S. Xiao, Y. F. Zhang, P. Guo, L. S. Zhong, X. P. Li and Z. Z. Zhang, *Catal. Today*, 2017, **281**, 327–336.
8 X. W. Nie, H. Z. Wang, M. J. Janik, Y. Chen, X. Guo and C. Song, *J. Phys. Chem. C*, 2017, **121**, 13164–13174.
9 T. Inoue, A. Fujishima, S. Konishi and K. Honda, *Nature*, 1979, **277**, 637–638.
10 D. O. Adekoya, M. Tahir and N. A. S. Amin, *J. CO2 Util.*, 2017, **349**, 218–225.
11 Y. Hori, K. Kikuchi and S. Suzuki, *Chem. Lett.*, 1985, 1695–1698.
12 S. Zhang, P. Kang, S. Ubnoske, M. K. Brennaman, N. Song, R. L. House, J. T. Glass and T. J. Meyer, *J. Am. Chem. Soc.*, 2014, **136**, 7845–7848.
13 B. Kumar, M. Asadi, D. Pisasale, S. Sinha-Ray, B. A. Rosen, R. Haasch, J. Abiade, A. L. Yarin and A. Salehi-Hhojin, *Nat. Commun.*, 2013, **4**, 2819.
14 S. Neatu, J. A. Macia-Agullo, P. Concepcion and H. Garcia, *J. Am. Chem. Soc.*, 2014, **136**, 15969–15976.
15 Y. P. Zhu, G. Chen, Y. J. Zhong, Y. B. Chen, N. N. Ma, W. Zhou and Z. P. Shao, *Nat. Commun.*, 2018, **9**, 2326.
16 Y. Hori, H. Wakebe, T. Tsukamoto and O. Koga, *Electrochim. Acta*, 1994, **39**, 2495–2500.
17 T. R. Zhuang, Z. Q. Liang, A. Seifitokaldani, Y. Li, P. D. Luna, T. Burdyny, F. L. Che, F. Meng, Y. M. Min, R. Quintero-Bermudez, C. T. Dinh, Y. J. Pang, M. Zhong, B. Zhang, J. Li, P. N. Chen, Z. L. Zheng, H. Y. Liang, W. N. Ge, B. J. Ye, D. Sinton, S. H. Yu and E. H. Sargent, *Nat. Catal.*, 2018, **1**, 421–428.
18 W. B. Hou, W. H. Hung, P. Pavaskar, A. Goeppert, M. Aykol and S. B. Cronin, *ACS Catal.*, 2011, **1**, 929–936.
19 X.-C. Ma, Y. Dai, L. Yu and B.-B. Huang, *Light: Sci. Appl.*, 2016, **5**, e16017.
20 W. Zhu, R. Michalsky, O. Metin, H. Lv, S. Guo, C. J. Wright, X. L. Sun, A. A. Peterson and S. Sun, *J. Am. Chem. Soc.*, 2013, **135**, 16833–16836.
21 F. Pincella, K. Isozaki and K. Miki, *Light: Sci. Appl.*, 2014, **3**, e133.

22 M. Schreier, F. Heroguel, L. Steier, S. Ahnmad, J. S. Luterbacher, M. T. Mayer, J. S. Luo and M. Gratzel, *Nat. Energy*, 2017, **2**, 17087.
23 S. Zhang, P. Kang, S. Ubnoske, M. K. Brennaman, N. Song, R. L. House, J. T. Glass and T. J. Meyer, *J. Am. Chem. Soc.*, 2014, **136**, 7845–7848.
24 B. Kumar, M. Asadi, D. Pisasale, S. Sinha-Ray, B. A. Rosen, R. Haasch, J. Abiade, A. L. Yarin and A. Salehi-Hhojin, *Nat. Commun.*, 2013, **4**, 2819.
25 T. Yang, X. Chang, J. Chen, K.-C. Chou and C. Hou, *Nanoscale*, 2015, **7**, 8955–8961.
26 Y. Wang, L. N. Zhang, X. Y. Zhang, Z. Z. Zhang, Y. C. Tong, F. Y. Li, J. C. S. Wu and X. X. Wang, *Appl. Catal., B*, 2017, **206**, 158–167.
27 J. P. Perdew, K. Burke and M. Ernzerhof, *Phys. Rev. Lett.*, 1996, **77**, 3865.
28 G. Kresse and D. Joubert, *Phys. Rev. B: Condens. Matter Mater. Phys.*, 1999, **59**, 1758.
29 N. W. Thibault, *Am. Mineral.*, 1944, **29**, 327–362.
30 D. D. Wang, D. X. Han, L. Liu and L. Niu, *J. Mater. Chem. A*, 2016, **4**, 14416–14422.
31 G. Henkelman, B. P. Uberuaga and H. Jónsson, *J. Chem. Phys.*, 2000, **113**, 9901.
32 G. Henkelman and H. Jónsson, *J. Chem. Phys.*, 2000, **113**, 9978.
33 Y. Toda, H. Hirayama, N. Kuganathan, A. Torrisi, P. V. Sushko and H. Hosono, *Nat. Commun.*, 2013, **4**, 2378.
34 S. Grimme, *J. Comput. Chem.*, 2006, **27**, 1787.

